ELECTROMAGNETICS LABORATORY
SCIENTIFIC REPORT NO. 86-5

May 1986

NEAR-FIELD SPILLOVER FROM A SUBREFLECTOR: THEORY AND EXPERIMENT

S. W. Lee**+
R. Acosta**
A. R. Cherrette**
P. T. Lam†

Supported by
Grant NAG3 - 419
NASA-Lewis Research Center
Cleveland, Ohio 44135

**Electromagnetics Laboratory
Department of Electrical and Computer Engineering
Engineering Experiment Station
University of Illinois at Urbana-Champaign
Urbana, Illinois 61801

+NASA-Lewis Research Center, Cleveland, Ohio 44135

†Lockheed Missiles and Space Company, Sunnyvale, California

UILU-ENG-86-2547

Electromagnetics Laboratory Report No. 86-5

NEAR-FIELD SPILLOVER FROM A SUBREFLECTOR: THEORY AND EXPERIMENT

by

S. W. Lee[**]
R. Acosta[+]
A. R. Cherrette[**]
P. T. Lam[†]

Scientific Report

May 1986

Supported by

Grant No. NAG3-419
NASA-Lewis Research Center
Cleveland, OH 44135

[**]Electromagnetics Laboratory
Department of Electrical and Computer Engineering
Engineering Experiment Station
University of Illinois at Urbana-Champaign
Urbana, Illinois 61801

[+]NASA-Lewis Research Center, Cleveland, Ohio 44135

[†]Lockheed Missiles and Space Company, Sunnyvale, California

~~Abstract~~

@ ABS

In a dual reflector antenna, the spillover from the subreflector is important in determining the accuracy of near-field measurements. This is especially so when some of the feed elements are placed far away from the focus. ~~In this paper, we present~~ A high-frequency GTD analysis of the spillover field over a plane just behind the subreflector is presented. Special attention is given to the field near the incident shadow boundary and the role played by the slope diffraction term. ~~Our~~ Computations are in excellent agreement with experimental results.

@ ABA Author

TABLE OF CONTENTS

LIST OF FIGURES

I. INTRODUCTION

Some dual-reflector antennas for space or radar applications have very large diameters in terms of wavelength (100 λ or more). They are usually tested in a near-field range. The far-field radiation patterns are extracted mathematically from the near-field measurement data. A typical near-field setup is sketched in Figure 1. The total field at a typical point C at the near-field recording plane consists of two contributions: the direct field from the main reflector (such as the field on ray ADEC), and the spillover from the subreflector. At high frequencies, the latter can be further decomposed into two components: the direct field from the feed on ray AC, and the edge diffracted from the rim of the subreflector on ray ABC. In many cases, the spillover is small, and, therefore, is traditionally neglected in near-field studies. However, there is an ever-increasing number of situations where the spillover must be taken into consideration. Two examples are:

(1) For an ultra-low sidelobe antenna, the wide-angle sidelobes are actually determined by the small spillover.

(2) To achieve a wide angle scan, many feed elements are placed away from the focus, and, consequently, the spillover is no longer small.

It is the purpose of this paper to study this spillover both theoretically and experimentally.

Referring to Figure 2, we shall derive a complete GTD analysis for the total diffracted field at a point C on the near-field recording plane. The feed location A is arbitrary and the subreflector surface is also arbitrary.

This analysis is very similar to one described in reference [1]. The difference is that, in the present analysis, the observation point C may fall on the incident shadow boundary (in contrast to the reflected shadow boundary in the analysis of [1]); therefore, uniform theories [2] - [4] must be used there.

In Sections II and III, an analysis is given for a simple configuration (hyperbolic reflector with a point feed at a focus). Nominal results presented in Section IV, however, include more general configurations.

II. SPECIAL CASE: HYPERBOLIC SUBREFLECTOR

The near-field calculation from a subreflector by GTD is very lengthy and tedious, because of the 3-D configuration and the arbitrariness in the feed and observation locations. We have developed a computer code for doing such a calculation. In the present section, let us concentrate on a special configuration, whose solution is simple enough to bring out the physical significance of various parameters.

The configuration is shown in Figure 3. A symmetrical hyperbolic subreflector is described by

$$z = f + b\sqrt{1 + \frac{x^2 + y^2}{f^2 - b^2}} \quad , \text{ for } x^2 + y^2 \leq a^2 \tag{2.1}$$

Here 2f is the distance between foci, 2b is that between vertices, and a is the radius of the circular aperature. The eccentricity of the hyperboloid is defined by f/b. The exterior wedge angle of the reflector is $m\pi$. For the special case in which m = 2, the wedge becomes a thin edge. The point feed is at a focus A. The incident field from it at an observation point (r, θ, ϕ = 0) is given by (for exp$j\omega t$ time convention)

$$\vec{E}^{i}(r, \theta, \phi = 0) = \frac{e^{-jkr}}{kr}\left[\theta P_{\theta}(\theta) + \phi P_{\phi}(\theta)\right] \tag{2.2}$$

Here $P_{\theta}(\theta)$ is the E-plane pattern and P_{ϕ} is the H-plane pattern of the feed. The problem at hand is to calculate the total field $\vec{E}^{t}$ at a near-field point C, whose conditions are (x = x, y = 0, z = c).

The parameters a, b, c, f, x, and m describe the geometry completely. For them, the following secondary geometrical parameters can be deduced (Figures 3 and 4):

Distances:
$$\ell_1 = [a^2 + (\ell_4 + 2f)^2]^{1/2} \tag{2.3}$$
$$\ell_2 = [(x - a)^2 + (c - \ell_4)^2]^{1/2}$$
$$\ell_3 = [x^2 + (c + 2f)^2]^{1/2}$$
$$\ell_4 = -f + b\sqrt{1 + \frac{a^2}{f^2 - b^2}}$$
$$\ell_5 = a(2f + c)/(2f + \ell_4)$$
$$\ell_6 = \ell_1(c - \ell_4)/(2f + \ell_4)$$

Diffraction angles:

$$\psi^{i} = [\mathrm{sgn}\ (\ell_5 - x)]\ \cos^{-1}\left[\frac{a(x - a) + (sf + \ell_4)(c - \ell_4)}{\ell_1 \ell_2}\right] \tag{2.4}$$

$$\psi^{r} = \pi - 2\theta_4 + \psi^{i}$$

$$\theta_4 = \cos^{-1}\frac{2f + \ell_4 - ag'}{\ell_1\sqrt{1 + g'^{12}}}$$

$$g' = \frac{ab}{\sqrt{(f^2 - b^2)(f^2 - b^2 + a^2)}}$$

Note that Ψ^i, defined in (2.4), obeys the following sign convention: Ψ^i is positive if observation point C is in the shadow region of $\vec{E}^i$, and is negative if C is in the lit region. For the present application, C is always in the shadow region of the reflected field $\vec{E}^r$ and, hence, Ψ^r defined in (2.4) is positive.

Let us now calculate the Keller's edge diffracted field $\vec{E}^d$ at C. There are two diffraction points: B and a corresponding point at the lower edge. In the present application, the lower edge is very weakly illuminated, and its contribution is therefore ignored. For the diffracted pencil emanated from b, the interfocal distance R calculated from Eq. (4.7) of [3] is

$$\frac{1}{R} = \frac{1}{\ell_1} + \frac{[(ag' - 2f - \ell_4)/\ell_1] + [c - \ell_4 + g'a - g'x)/\ell_2]}{a\sqrt{1 + g'^2}} \tag{2.5}$$

The diffraction coefficients as calculated from Eq. (4.10) of [3] are

$$\chi^{i,r} = \frac{\frac{2}{m}\sin\frac{\pi}{m}}{\cos\frac{\pi}{m} - \cos\frac{\pi + \psi^{i,r}}{m}} \tag{2.6}$$

The diffracted field at C is calculated from Eq. (4.8) of [3]. The final result is

$$\begin{aligned}\vec{E}^d(C) = {} & \frac{e^{-j(k\ell_2+\pi/4)}}{2\sqrt{2\pi k\ell_2}} \frac{1}{\sqrt{1 + (\ell_2/R)}} \\ & \cdot \left[\left(\hat{x}\,\frac{C - \ell_4}{\ell_2} - \hat{z}\,\frac{n - a}{\ell_2}\right)(\chi^i + \chi^r)\, E^i_\theta(B)\right. \\ & \left. + \hat{y}\,(\chi^i - \chi^r)\, E^i_\phi(B)\right]\end{aligned} \tag{2.7}$$

where

$$\begin{bmatrix} E_\theta^i(B) \\ \\ E_\phi(B) \end{bmatrix} = \frac{e^{-jk\ell_1}}{k\ell_1} \begin{bmatrix} P_\theta(\theta_1) \\ \\ P_\phi(\theta_1) \end{bmatrix}$$

$$\theta_1 = \sin^{-1}(a/\ell_1)$$

According to UAT [3], the total field $\vec{E}^t$ at C is the sum of the Keller's diffracted field $\vec{E}^d$ in (2.7) and a modified geometrical optics field $\vec{E}^G$ such that

$$\text{UAT:} \quad \vec{E}^t(C) = \vec{E}^G(C) + E^d \tag{2.8}$$

Here $\vec{E}^G$ is given by

$$\vec{E}^G(C) = [F(\zeta) - \hat{F}(\zeta)]\, \vec{E}^i(C) \tag{2.9}$$

The detour parameter is defined by

$$\zeta = \text{sgn}(\ell_5 - x)\, \left|\sqrt{k(\ell_1 + \ell_2 - \ell_3)}\right| \tag{2.10}$$

The Fresnel function is defined by

$$F(x) = \frac{e^{j\pi/4}}{\sqrt{\pi}} \int_x^\infty e^{-jt^2}\, dt \tag{2.11}$$

Its leading asymptotic expansion for $x \to \infty$ is

$$\hat{F}(x) = \frac{1}{2x\sqrt{\pi}} \exp[-j(x^2 + \tfrac{\pi}{4})] \tag{2.12}$$

A polynominal approximation of F(x) is, for x > 0,

$$F(-x) = 1 - F(x) \tag{2.13a}$$

$$F(x) \approx \frac{1}{2}e^{-jx^2}\,[(f_1 + f_2) - j(f_1 - f_2)] \tag{2.13b}$$

where

$$f_1(x) = (1 + 0.739x)/(2 + 1.430x + 1.976x^2)$$

$$f_2(x) = 1/(2 + 3.305x + 2.223x^2 + 3.388x^3)$$

In summary, for the diffraction problem in Figure 3, the total field at C is given by (2.8). This solution is derived based on UAT, and is valid for observation points on line CD, including the transition region around the incident boundary D.

III. FIELD ON INCIDENT SHADOW BOUNDARY

For the hyperbolic reflector in Figure 3, let us calculate the total field at D, the point exactly on the incident shadow boundary. In the absence of the reflector, the incident field from the source at point A is given by (Figure 5)

$$\vec{E}^i(D) = \frac{e^{-jk(\ell_1+\ell_6)}}{k(\ell_1+\ell_6)}\,[\hat{\theta}P_\theta(\theta_1) + \hat{\phi}P_\theta(\theta_1)] \tag{3.1}$$

$$= \hat{\theta}E^i_\theta(D) + \hat{\phi}E^i_\theta(D)$$

When the reflector is present, the total field $\vec{E}^t(D)$ can be calculated from (2.8). Both $\vec{E}^G$ and $\vec{E}^d$ become singular at D, but their singularities cancel each other. The total field is finite and continuous there. Omitting the

derivations, we give the final results below. For the θ-component (component perpendicular to the edge), the normalized total field at D is

$$\text{VAT:}\quad \frac{E_\theta^t(D)}{E_\theta^i(D)} = A_0 + \frac{e^{-j\pi/4}}{2\sqrt{2\pi k \ell_6 (1+\ell_6/\ell_1)}}\,[A_1 + A_2 + A_3] \tag{3.2}$$

where

$$A_0 = \frac{1}{2}$$

$$A_1 = 2(\ell_6/\ell_1)\; P'_\theta(\theta_1)/P_\theta(\theta_1)$$

$$A_2 = (\ell_6/\ell_1)\cot\theta_1 - [1 + (\ell_6/\ell_1)]\,\frac{1}{m}\cot\frac{\pi}{m}$$

$$A_3 = \chi^r[1 + (\ell_6/\ell_1)]$$

$$P'_\theta(\theta) = d\,P_\theta(\theta)/d\theta$$

The diffraction coefficient χ^r is defined in (2.6) and diffraction angle ψ^r in (2.4). For the φ-component (component parallel to the edge), the same expression (3.2) holds except for the following replacements:

$$E_\theta^{i,t} \to E_\phi^{i,t},\quad P_\theta \to P_\theta,\quad \chi^r \to (-1)\chi^r \tag{3.3}$$

Several remarks about the solution in (3.2) are in order.

(i) Solution (3.2) is a high-frequency asymptotic solution, accurate only to the order of $k^{-1/2}$.

(ii) The solution is not valid if observation point D approaches edge point B. It does not satisfy the proper edge condition at B.

(iii) The dominant term A_0 in (3.2) gives one half of the incident field, a well-known fact. The remaining terms are of order $k^{-1/2}$. Their contribution decreases as the source point A moves away from the edge ($\ell_1 \to \infty$).

(iv) The term A_1 is proportional to the angular slope of the pattern function $P_\theta(\theta)$ of the incident field. It is sometimes known as the slope diffraction contribution.

(v) If UTD [4] is applied to the problem in Figure 4, the corresponding solution again has the form of (3.2) except that terms A_1 and A_2 are absent*.

Let us present some numerical results calculated from (3.2). The subreflector parameters are (Figure 3)

$$a = 12\lambda,\ b = 5\lambda,\ f = 12\lambda$$

Some deduced parameters are (Figure 4 is to scale)

$$\ell_1 = 22.8\lambda \quad , \quad m\pi = 360° - 18.7° = 1.8961\ \pi \tag{3.4}$$
$$\theta_1 = 31.7° \quad , \quad \psi^r = 79.14°$$

---

*The slope diffraction coefficient d_s (or d_h) in Eq. (7) of [5] cannot be used to calculate the field on the incident shadow boundary, because d_s is undefined there. This is due to the fact that D_s of UTD has a step discontinuous across the incident shadow boundary in order to cancel the step discontinuity of the geometrical optics field. The angular derivative of D_s does not exist there.

The pattern of the incident field is assumed to be

$$P_\theta(\theta) \text{ or } P_\phi(\theta) = [\cos(\theta - \theta_0)]^{20} \tag{3.5}$$

where $\theta = \theta_0$ is the main beam direction. The 3 dB beamwidth of the incident beam is 21.3°. Thus, instead of a local plane wave, the magnitude of the incident field has a rapid angular variation.

Figure 6 shows the importance of the slope diffraction term A_1 in (3.2). For the present case, A_1 reads

$$A_1 = 2(\ell_6/\ell_1)\ (20)\ \tan(\theta_0 - \theta_1) \tag{3.6}$$

When $\theta_0 = \theta_1 = 31.7°$, term A_1 is zero and we find

$$\frac{E^t_\theta(D)}{E^i_\theta(D)} = 0.573e^{-j6.9°} \tag{3.7a}$$

$$\frac{E_\phi(D)}{E^i_\phi(D)} = 0.458e^{+j5.6°} \tag{3.7b}$$

Had the slope diffraction been ignored, the total field would have been given by (3.7) for all values of beam direction θ_0. Figure 6 shows that the normalized field increases indefinitely as the beam sweeps from the shadow side to the lit side. When $\theta_0 = 90° + \theta_1$, the incident field $E^i_\theta(D)$ or $E^i_\phi(D)$ is zero in accordance with (3.5), but the total field at D is not zero. Hence, the normalized field is infinite.

In Figure 7, the incident beam is displaced by one beamwidth (21.3°) on either side of the shadow boundary. Note that the field is stronger when

the beam is displaced to the lit side. When the observation point D moves far away from the edge, solution (3.2) approaches its far-field value, namely,

$$\frac{E_\theta^t(D)}{E_\theta^i(D)} = \frac{1}{2} + \frac{e^{-j\pi/4}}{2\sqrt{2\pi k \ell_1}} \left(2\frac{P_\theta^1}{P_\theta} + \cot\theta_1 - \frac{1}{m}\cot\frac{\pi}{m} + \chi^r\right) \quad , \quad (\ell_6/\ell_1) \to \infty \tag{3.8}$$

This asymptotic behavior can be seen from Figure 7.

IV. NUMERICAL RESULTS AND EXPERIMENTS

Parameters of the experimental hyperbolic reflector are (Figure 8)

$$a = 50.54" \quad , \quad b = 23.39" \quad , \quad f = 24.32" \tag{4.1}$$

Eccentricity = f/b = 1.04

There are two feeds: one for 20 GHz (λ = 0.59") and the other for 30 GHz (λ = 0.39"). Their E-plane patterns $P_\theta(\theta)$ and the H-plane patterns $P_\phi(\theta)$ are described by

$$[\cos(\theta - \theta_0)]^q \tag{4.2}$$

where $\theta_0 = 43.5°$. Thus, the beam is 8° displaced from the incident shadow boundary. The values of q and beamwidths are

	q		3 dB beamwidth	
	E-plane	H-plane	E-plane	H-plane
20 GHz	125	69	8.5°	11.5°
30 GHz	136	125	8.2°	8.5°

(4.3)

The fields behind the subreflector over a planar surface were measured at the NASA-Lewis near-field facility. Corresponding theoretical values are calculated from (2.8), (2.9), and (2.7). Results are presented in Figures 9 to 11. The agreement between theory and experiment is excellent.

The computer program used to calculate the theoretical values is quite general. As an example consider the modified subreflector-feed geometry shown in Figure 12. Here the feed has been moved up 12 inches in the y-direction and repointed along the incident shadow boundary. The feed pattern half-power beam width has also been increased to 42.2°. Figure 13 depicts the amplitude of E_x for this set of conditions at 30 GHz.

V. CONCLUSION

(1) Based on UAT, we have developed a near-field spillover analysis for an arbitrarily shaped subreflector with a feed at an arbitrary location (Figure 2). A typical result is shown in Figure 12.

(2) For the special case in which the subreflector is hyperbolic and the feed is on focus, explicit solutions are given in Sections II and III. The total field at the observation point C in Figure 3 is given in (2.8), (2.9), and (2.7).

(3) Special attention is given to the field at point D (Figure 5) on the incident shadow boundary. As described in (3.2), the slope diffraction term A_1 plays an important role when the incident beam has a rapidly varying pattern.

(4) An excellent agreement is obtained between the theoretical and the measured results (Figures 9 to 11) for fields just behind a large hyperbolic subreflector, which is illuminated by a field with a rapid angular variation.

REFERENCES

[1] S. W. Lee, P. Cramer, Jr., K. Woo, and Y. Rahmat-Samii, "Diffraction by an arbitrary subreflector: GTD solution," IEEE Trans. Antennas Propagat., vol. AP-27, pp. 305-316, 1979. See also correction in AP-34, p. 272, 1986.

[2] D. S. Ahluwalia, R. M. Lewis, and J. Boersma, "Uniform asymptotic theory of diffraction by a plane screen," SIAM J. Appl. Math., vol. 16, pp. 783-807, 1968.

[3] S. W. Lee and G. A. Deschamps, "A uniform asymptotic theory of electromagnetic diffraction by a curved wedge," IEEE Trans. Antennas Propagat., vol. AP-24, pp. 25-34, 1976.

[4] R. G. Kouyoumijian and P. H. Pathak, "A uniform geometrical theory of diffraction for an edge in a perfectly-conducting surface," Proc. IEEE, vol. 62, pp. 1448-1461, Nov. 1974.

[5] R. G. Kouyoumijian and P. H. Pathak, "Reply to a comment by J. D. Cashman," IEEE Trans. Antennas Propagat., vol. AP-25, pp. 447-451, 1977.

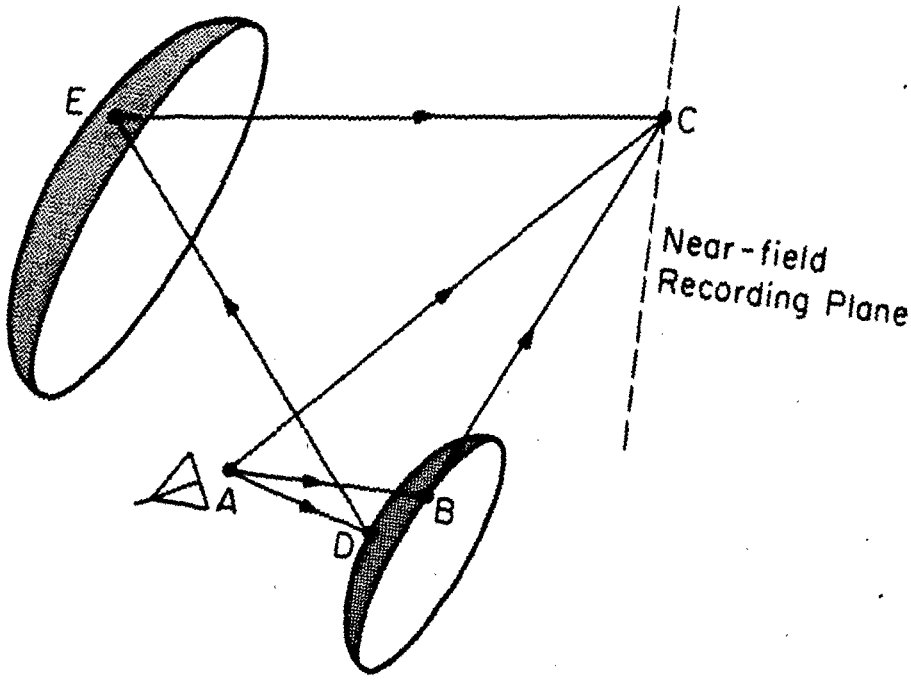

Figure 1. Near-field measurement of radiation from a dual-reflector antenna.

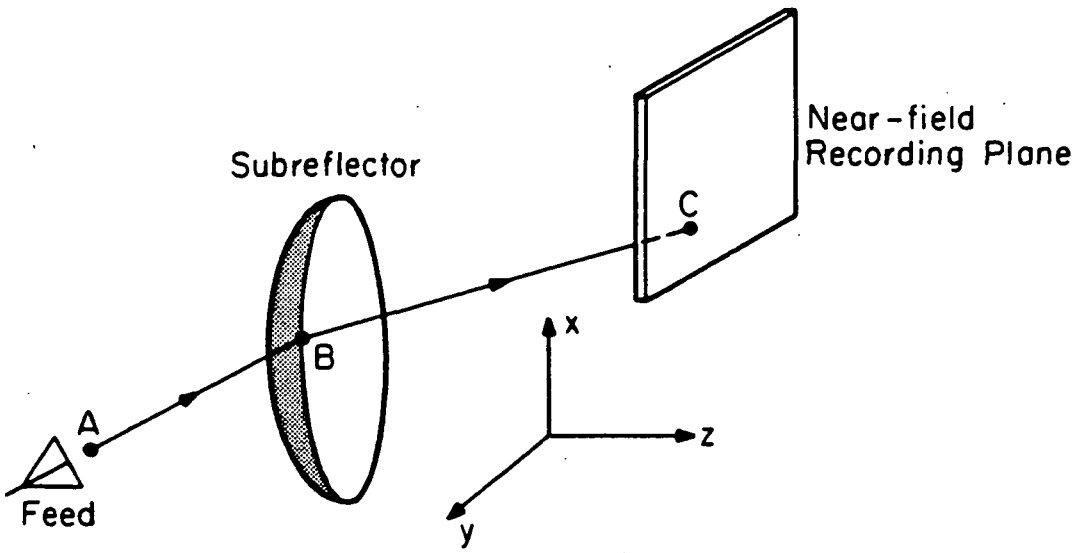

Figure 2. Near-field diffraction by an arbitrary subreflector.

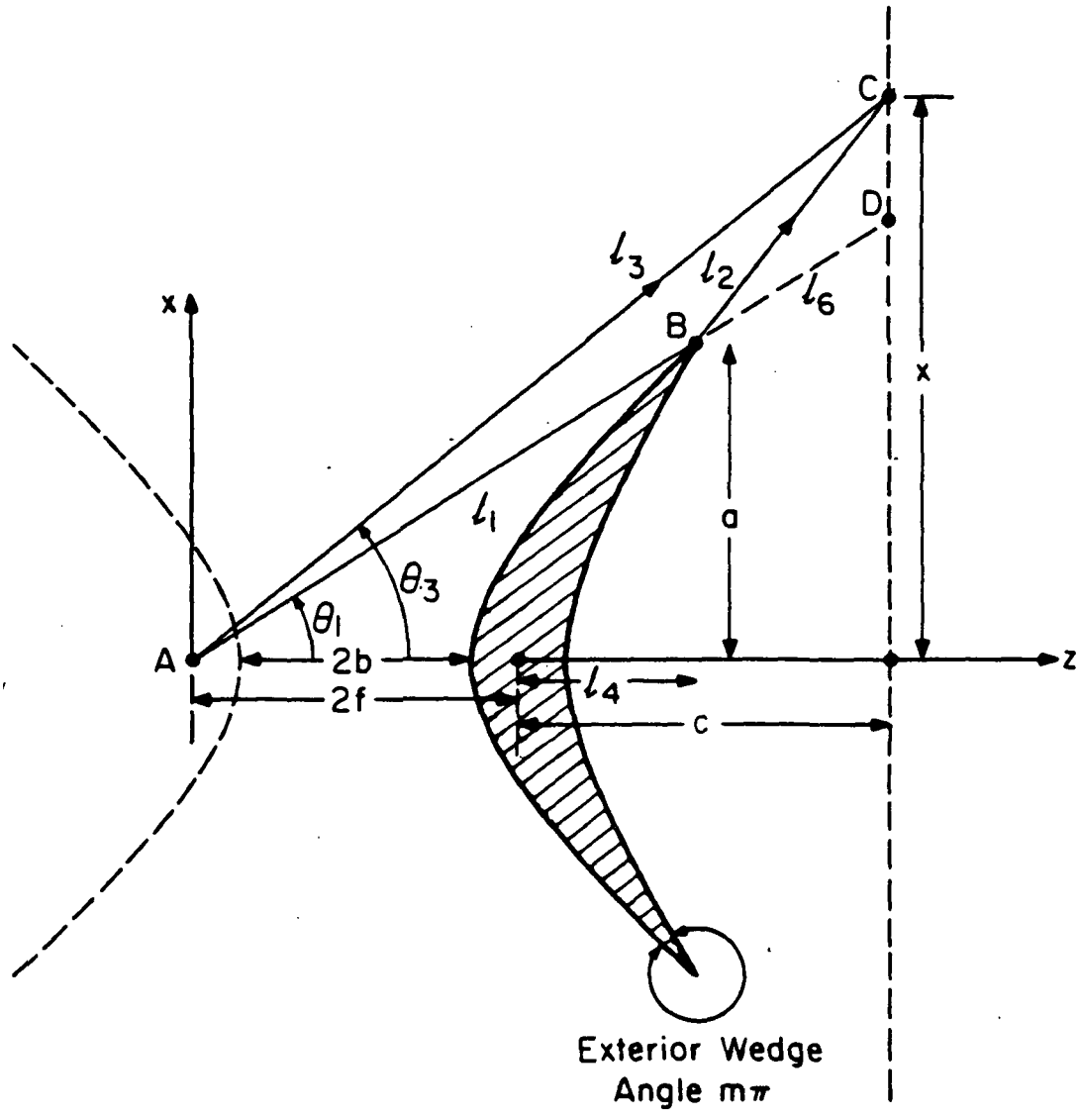

Figure 3. A hyperbolic subreflector with rotating symmetry about z-axis. The radius of the circular aperture is a.

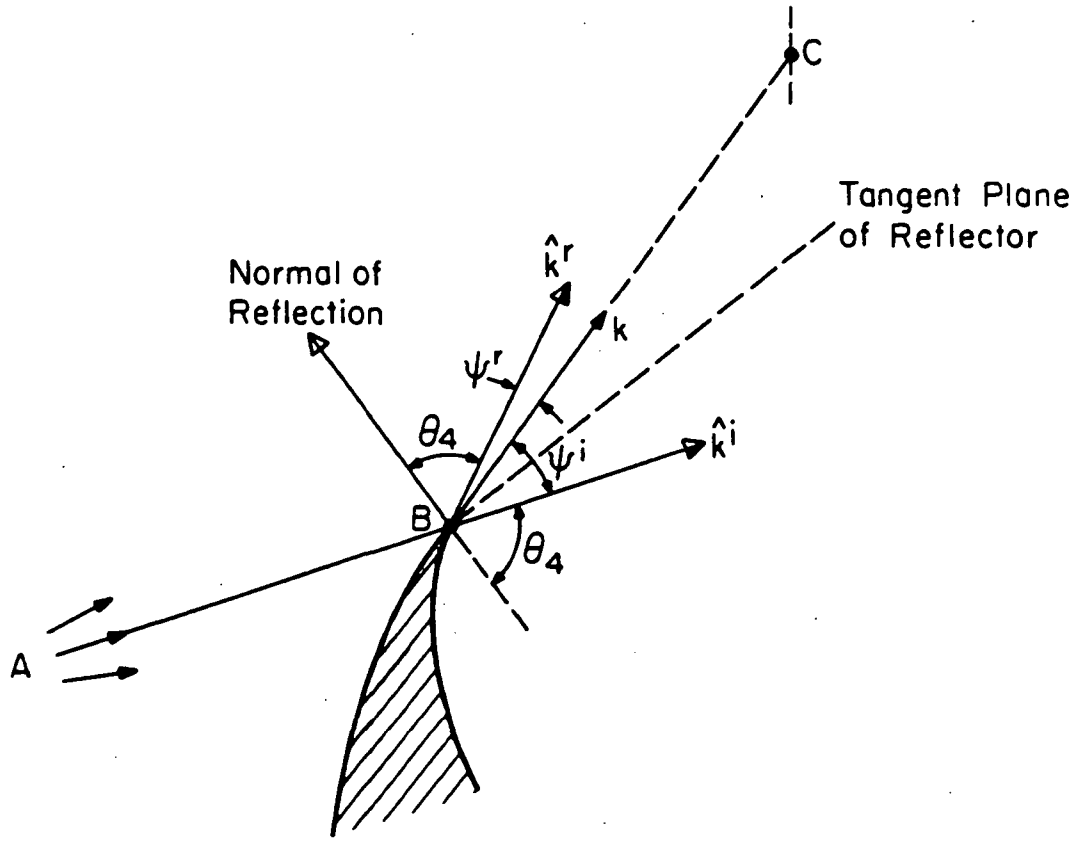

Figure 4. Diffraction angles ψ^i and ψ^r. Dark half of arrow $\hat{k}^i$ (or $\hat{k}^r$) indicates shadow side of $\vec{E}^i$ (or $\vec{E}^r$).

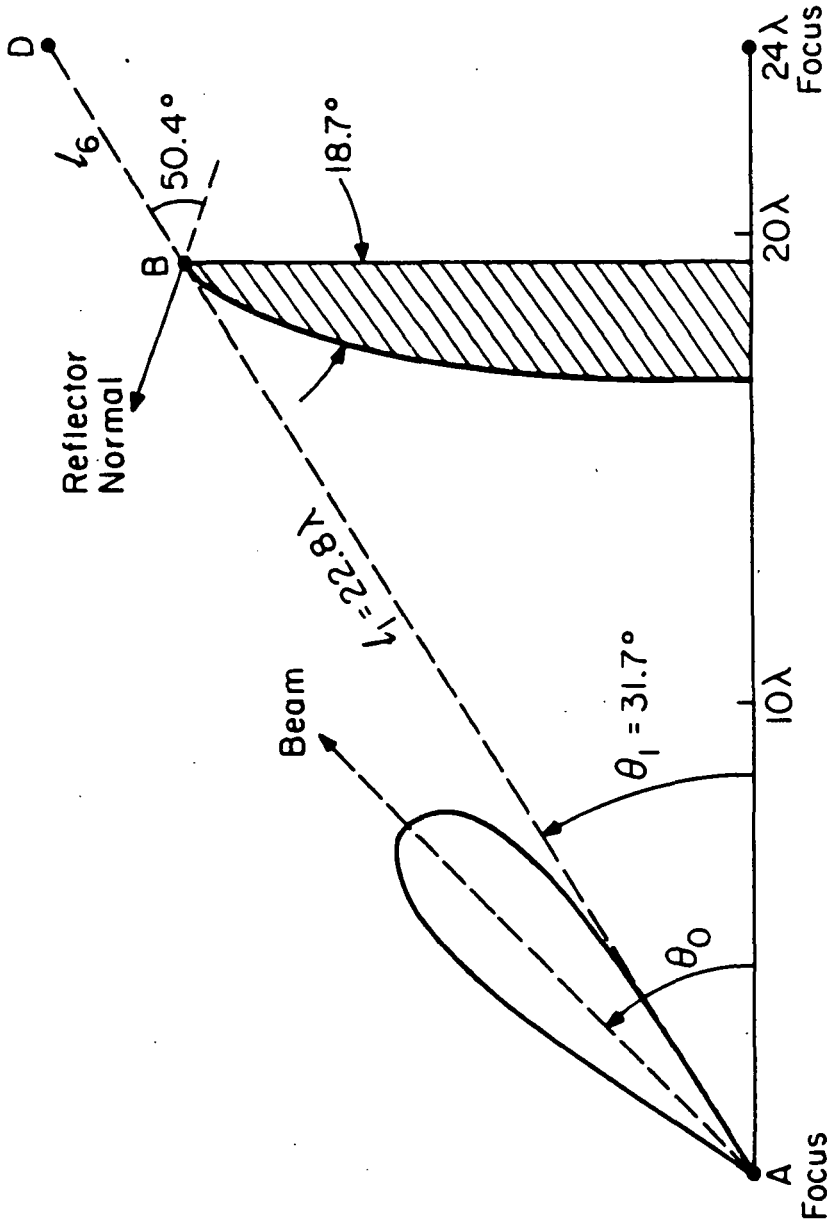

Figure 5. Field at D on the incident shadow boundary for a hyperbolic subreflector illuminated by a source at focus A.

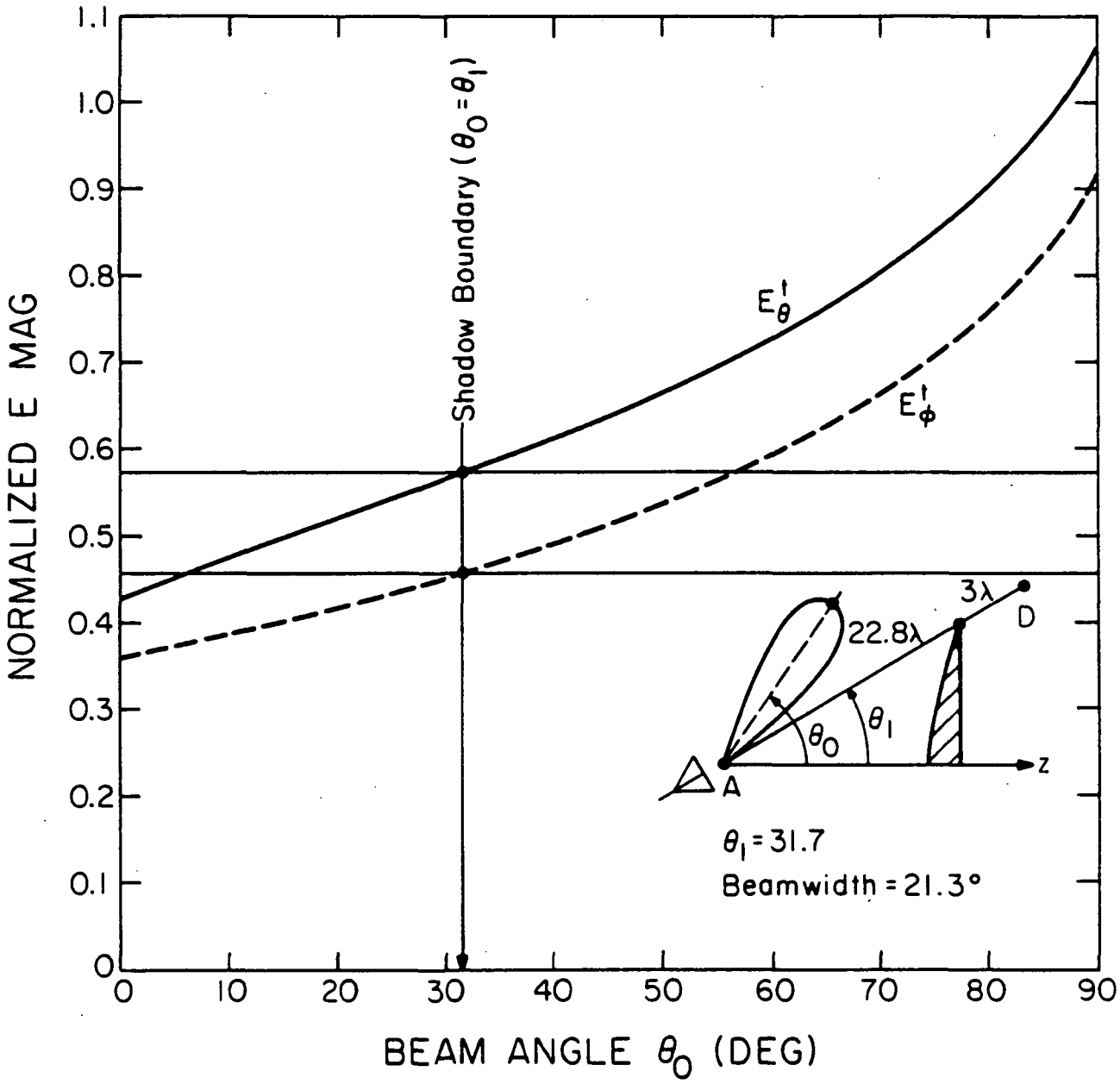

Figure 6. Total field at point D on the incident shadow boundary, normalized with respect to the incident field at D for the configuration in Figure 5.

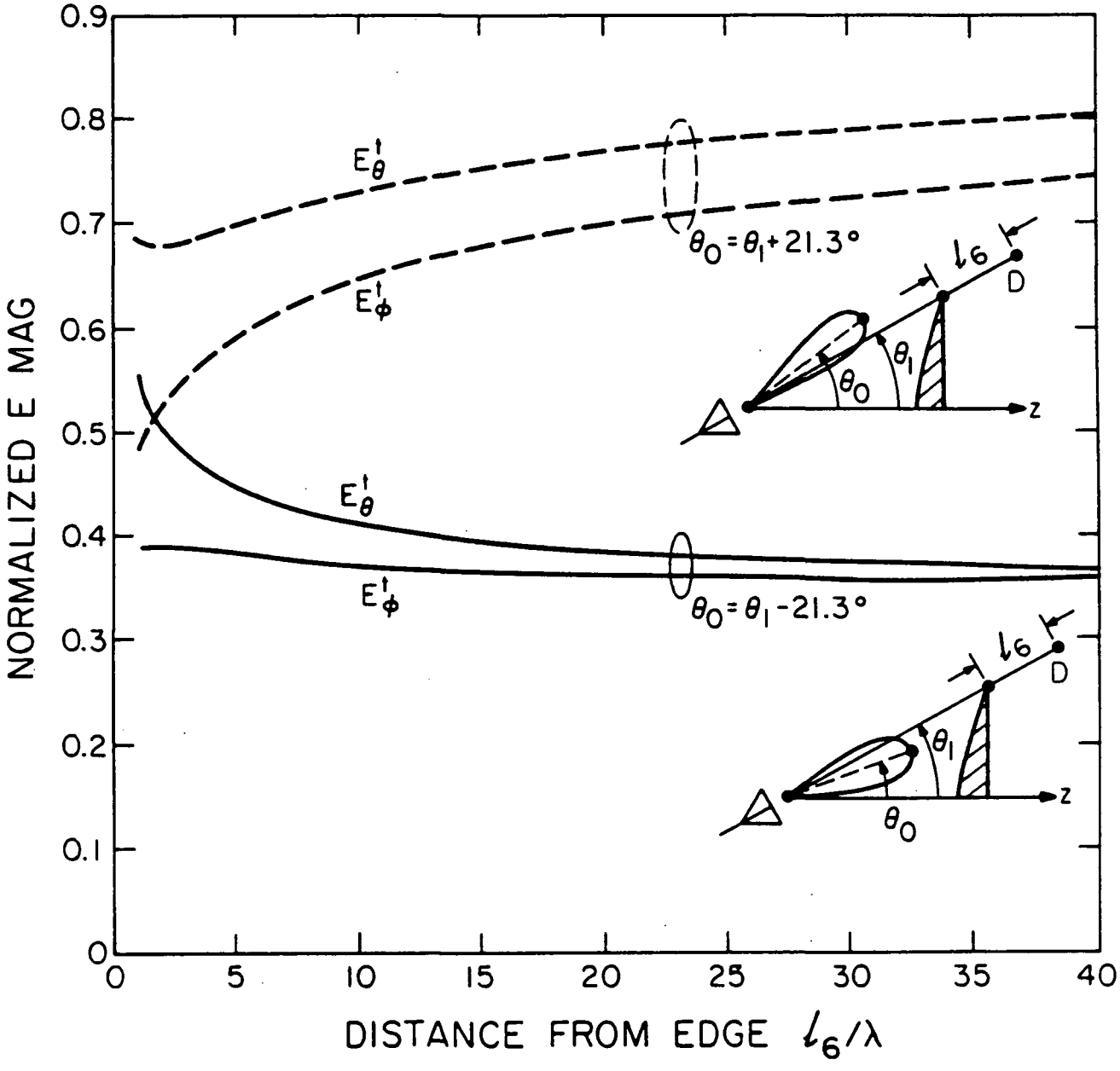

Figure 7. Total field at point D on the incident shadow boundary, normalized with respect to the incident field at D for configuration in Figure 5. Incident beam direction is displaced by one beamwidth (21.3°) on either side of the shadow boundary.

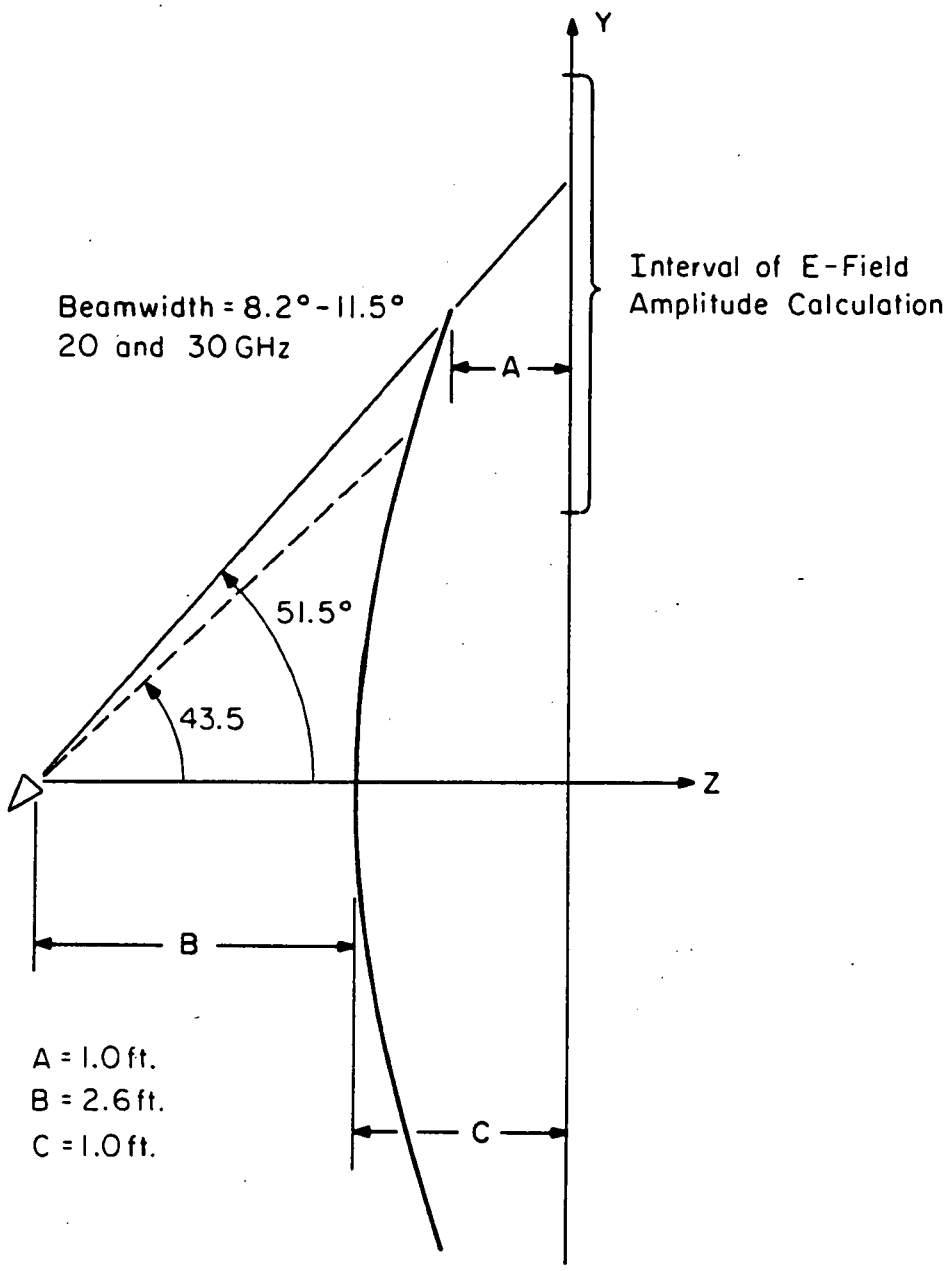

Figure 8. Hyperbolic subreflector used in a NASA-Lewis experiment.

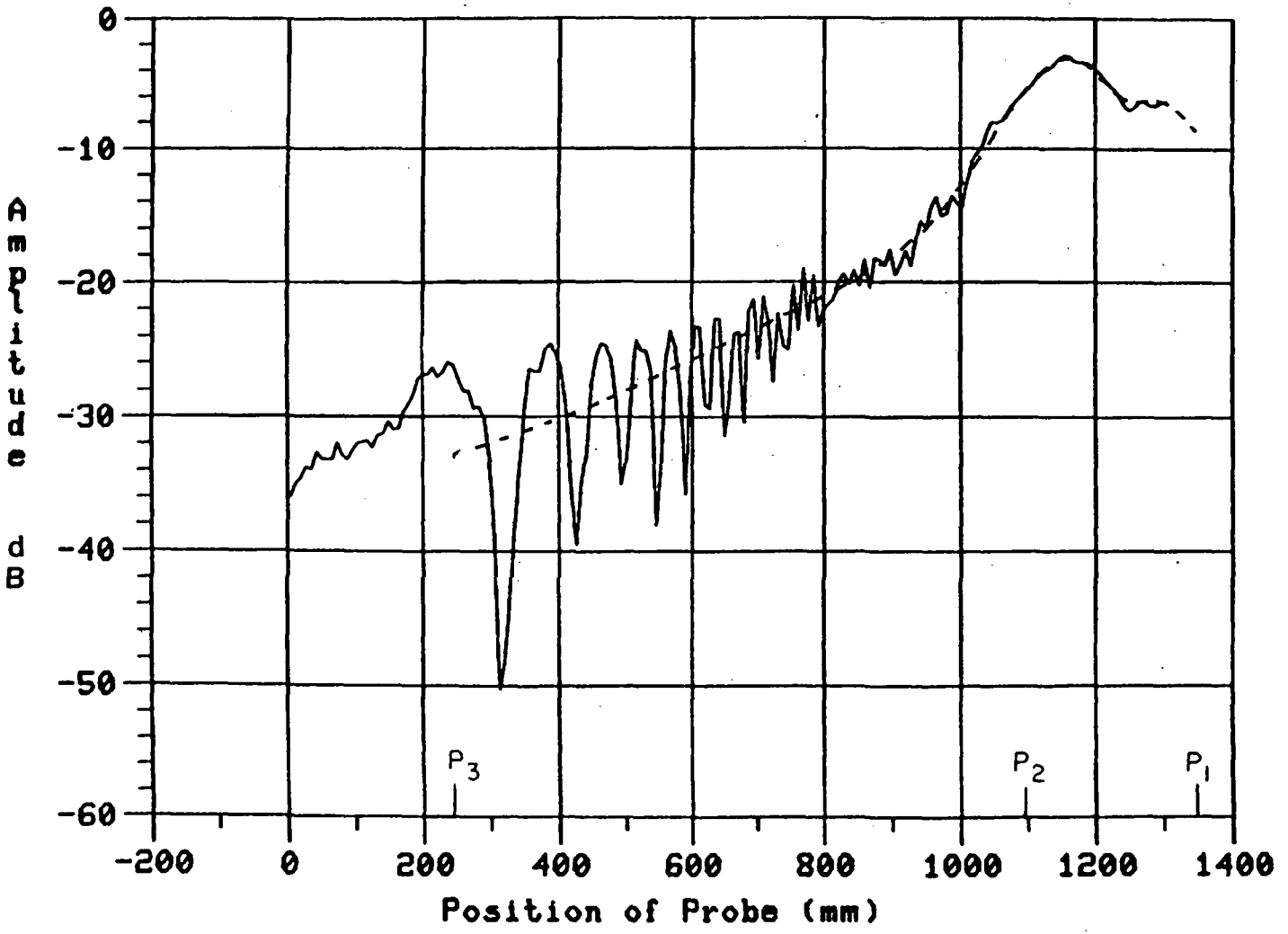

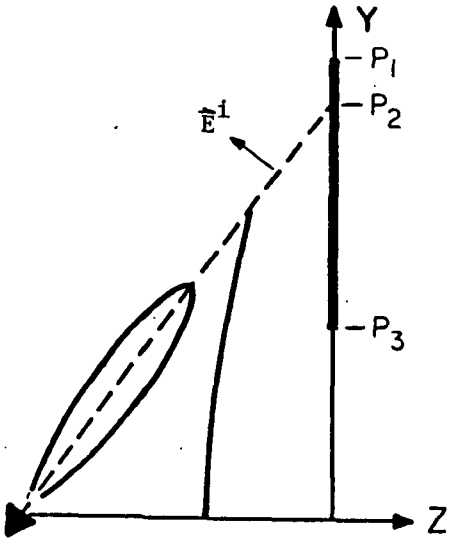

20 GHz, E_x

----- Theory

—— Measured

Figure 9a. Near-field E-plane diffraction pattern (E_x component) at 20 GHz for the configuration in Figure 8.

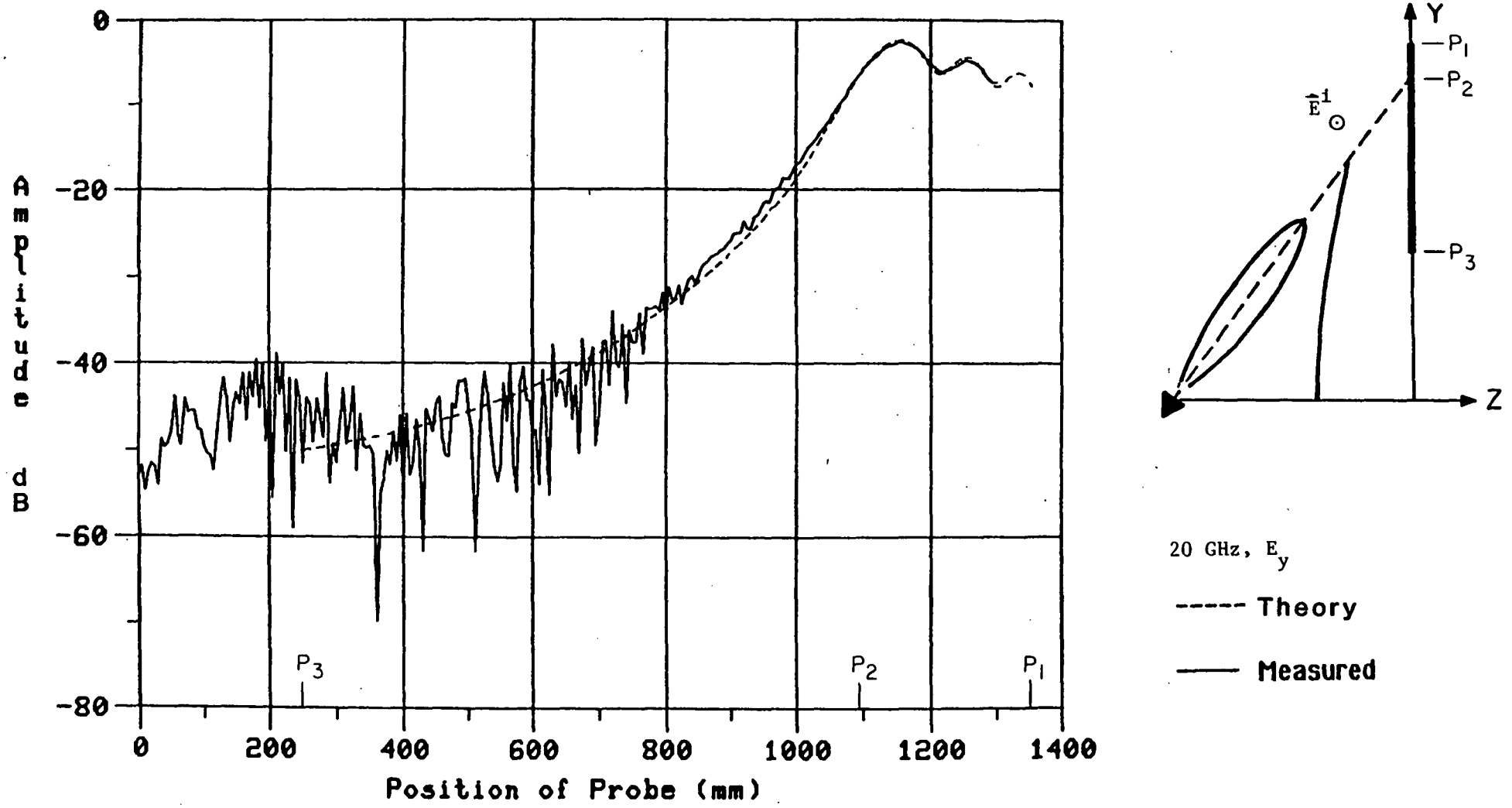

Figure 9b. Same as Figure 9a except for H-plane diffraction pattern (E_y component).

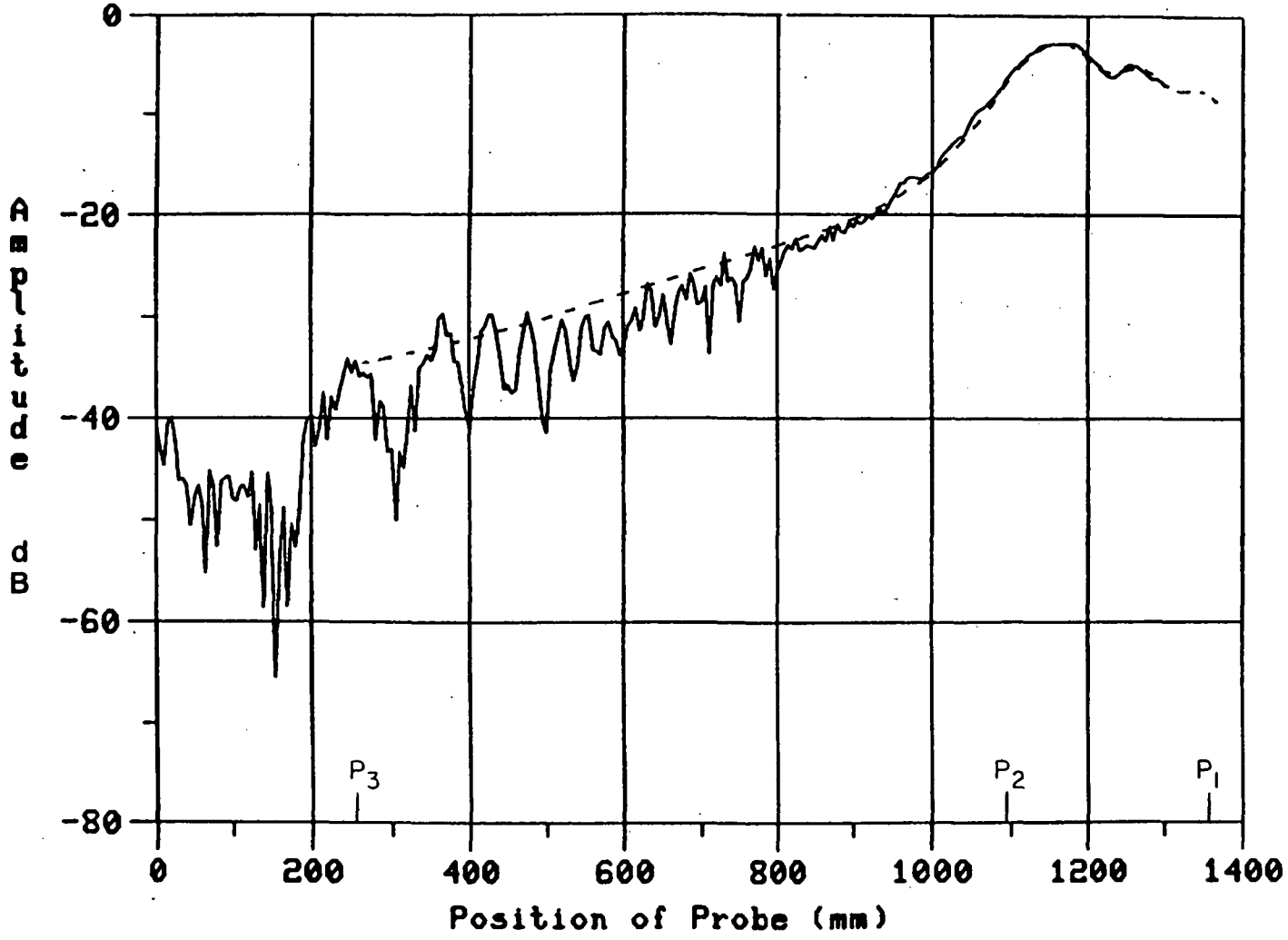

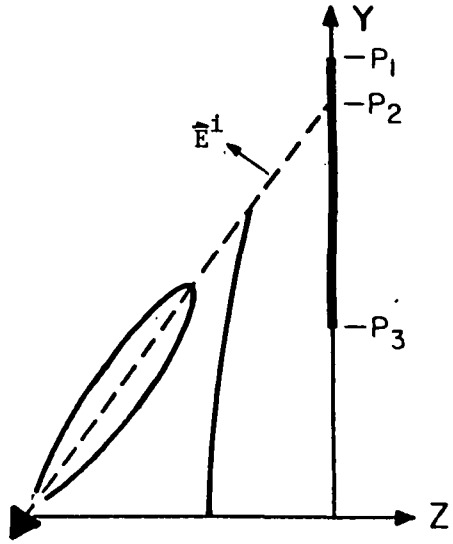

30 GHZ, E_x

----- Theory

—— Measured

Figure 10a. Near-field E-plane diffraction pattern (E_x component) at 30 GHz for the configuration in Figure 8.

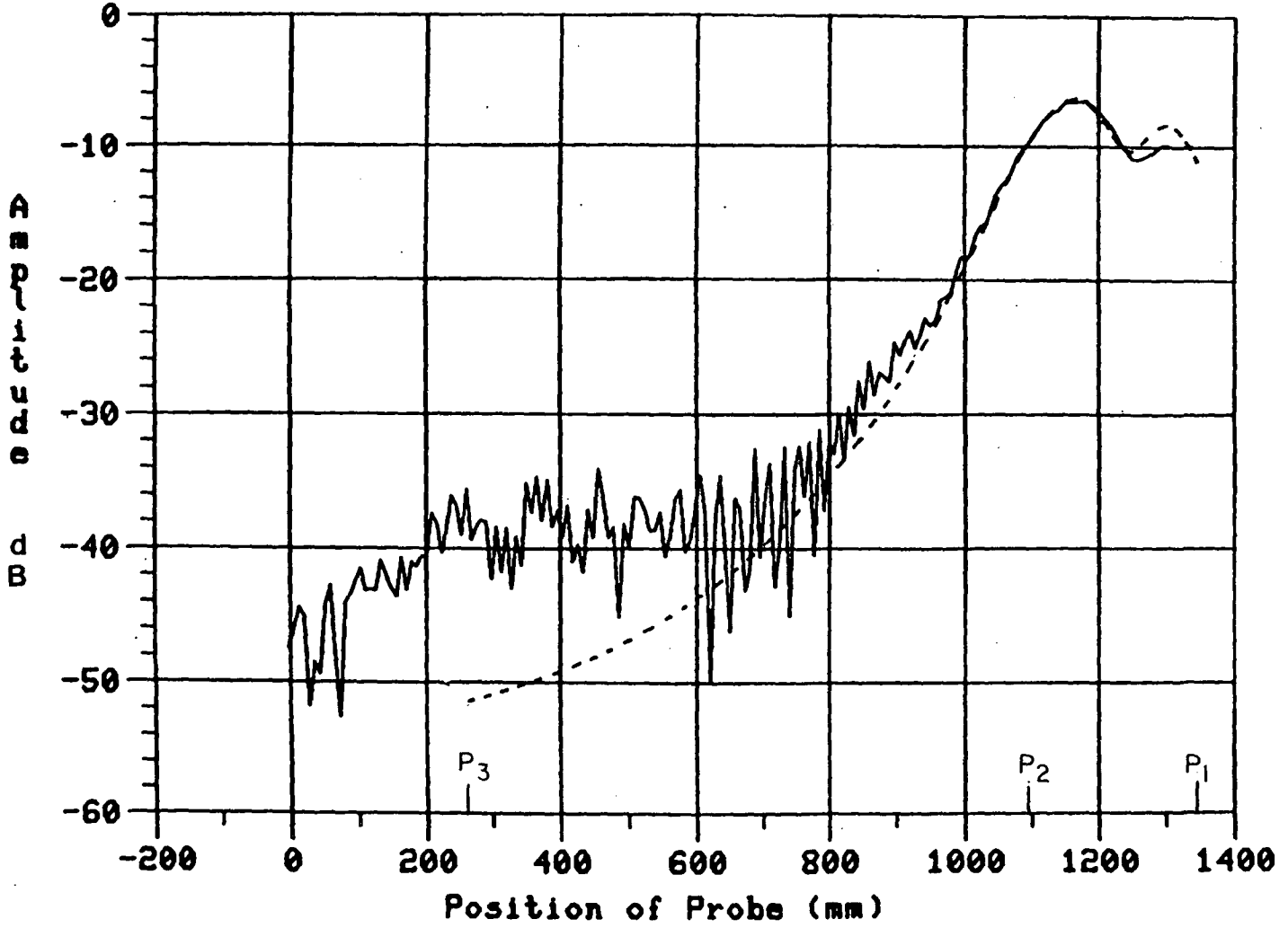

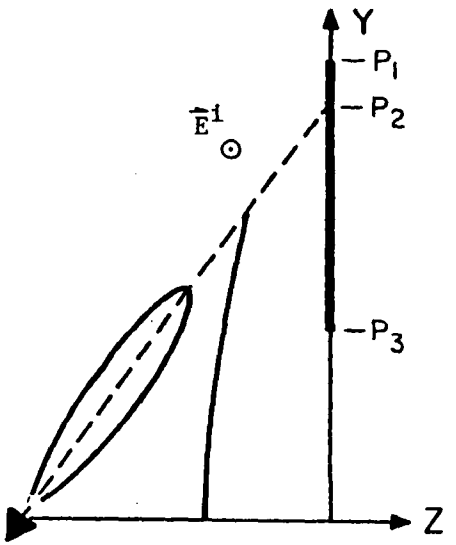

30 GHz, E_y

----- Theory

—— Measured

Figure 10b. Same as Figure 10a except for H-plane diffraction pattern (E_y component).

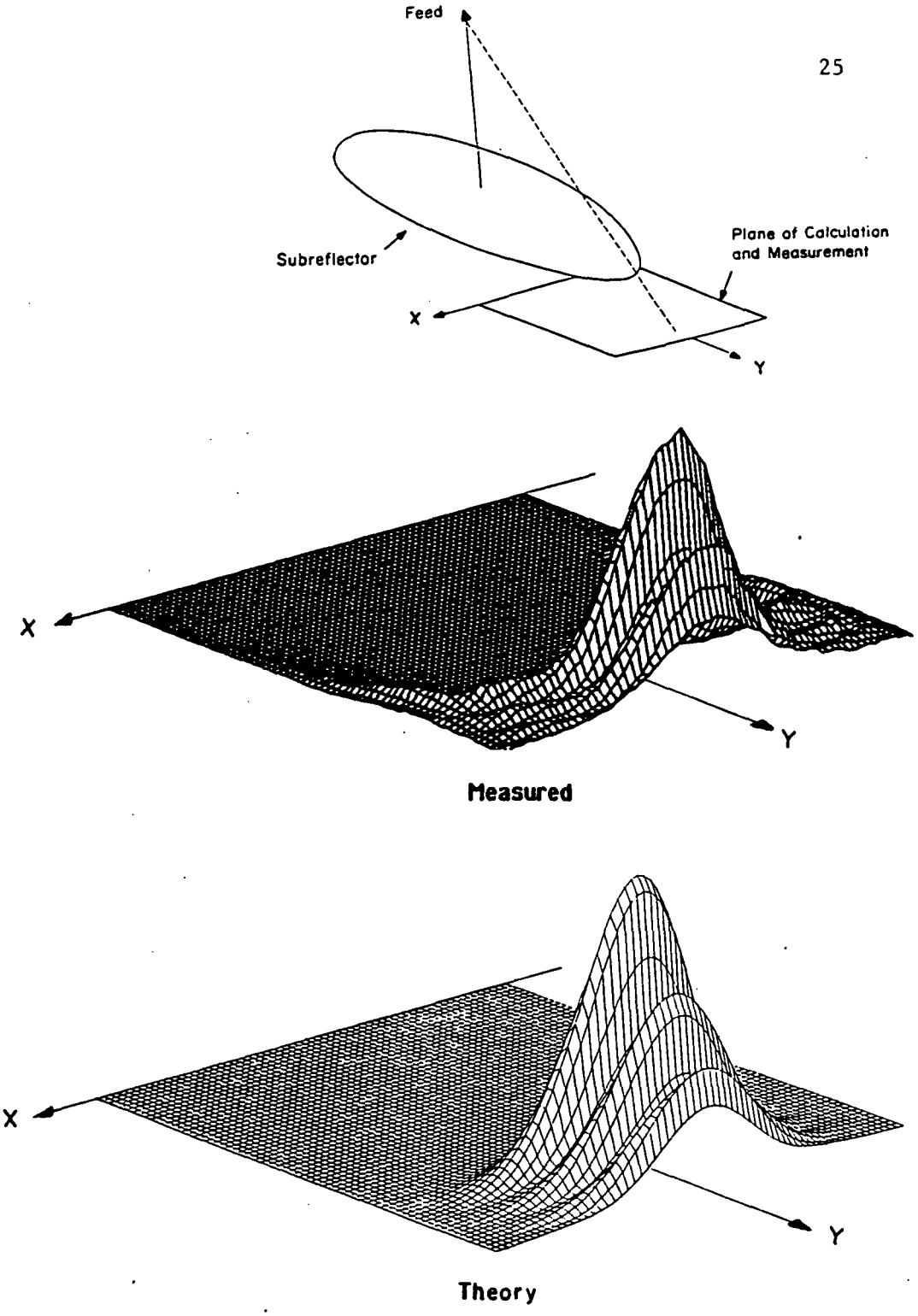

Figure 11. Near-field diffraction pattern of the subreflector in Figure 8 when it is illuminated by a feed polarized in the y-direction at 30 GHz.

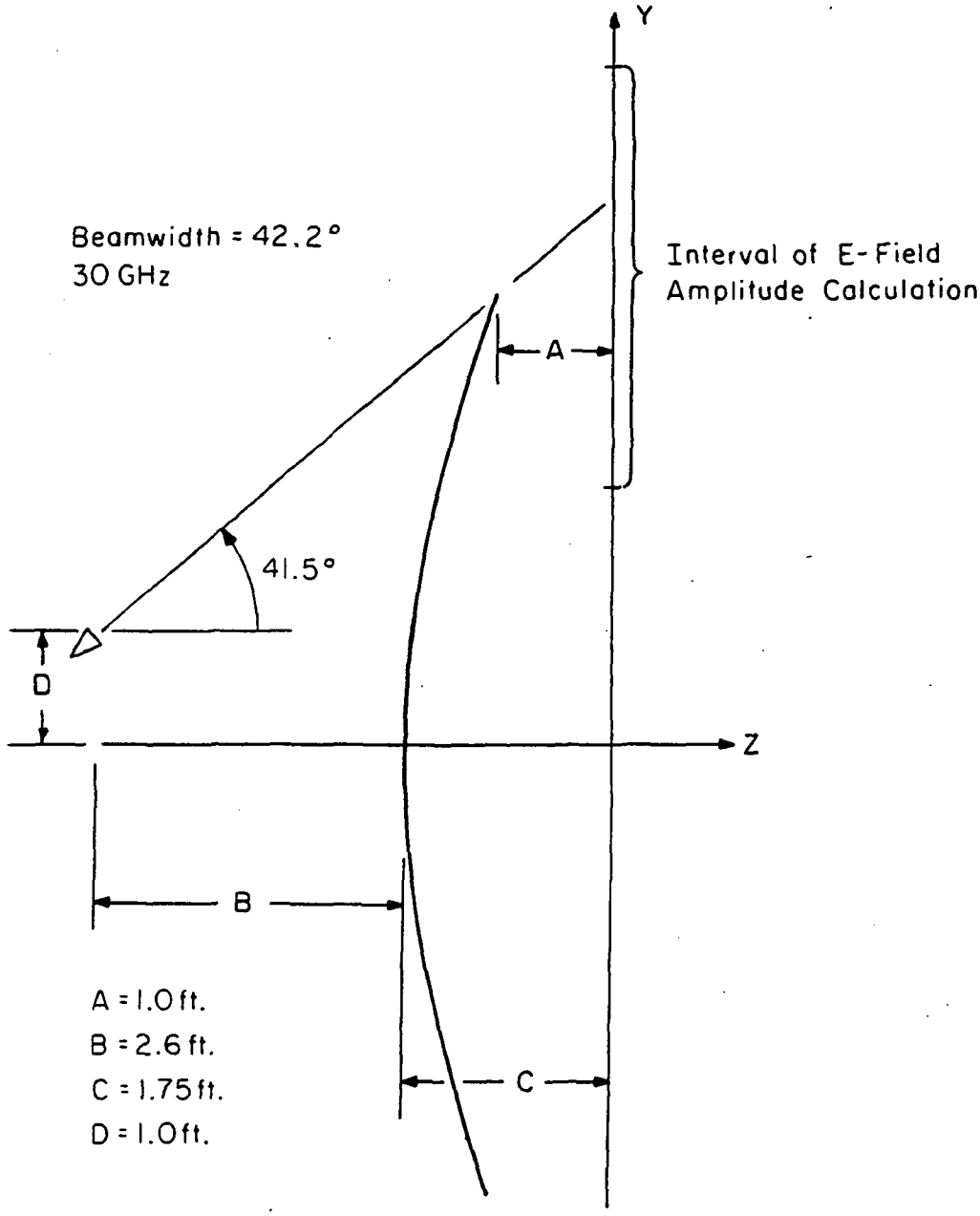

Figure 12. Modified hyperbolic subreflector geometry.

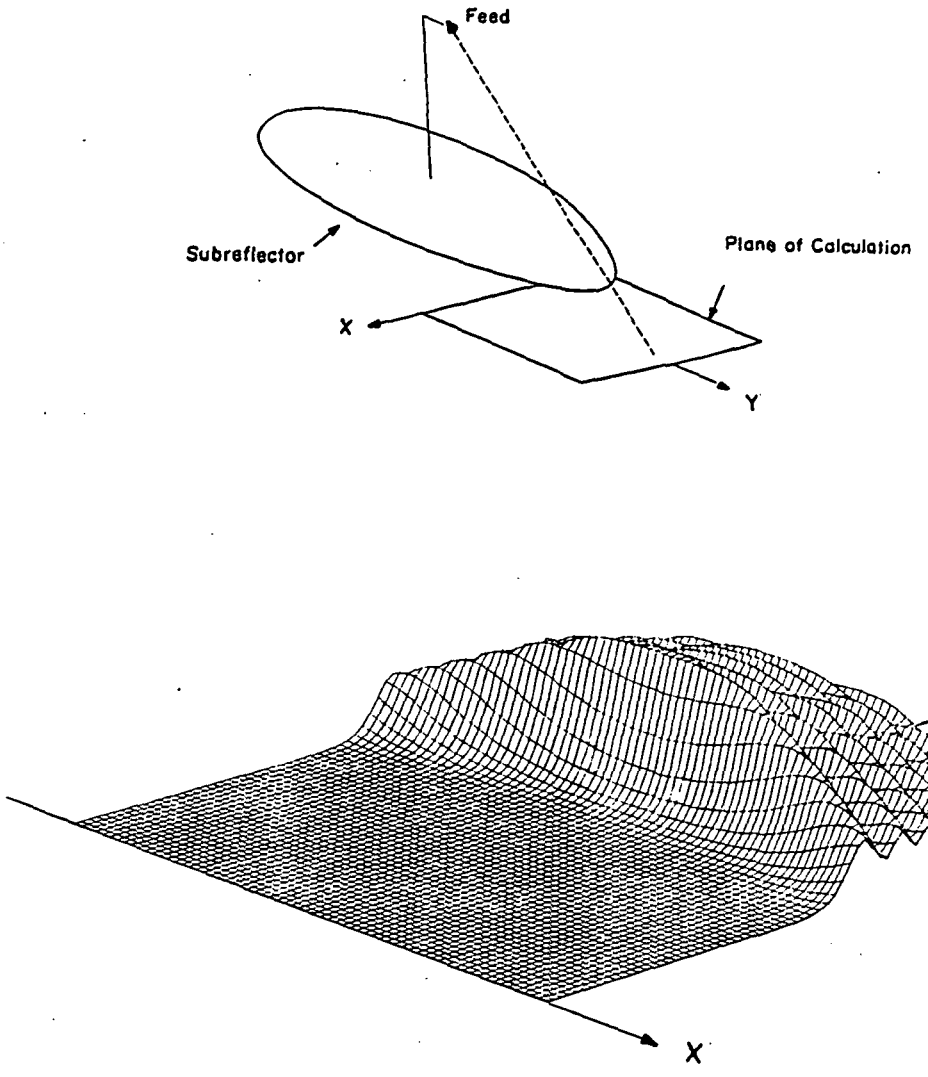

Figure 13. Calculated near-field diffraction pattern of the subreflector in Figure 12 when it is illuminated by a feed polarized in the x-direction.